A large-area, position-sensitive neutron detector with neutron/γ-ray discrimination capabilities

P.D. Zecher[a,*], A. Galonsky[a], J.J. Kruse[a], S.J. Gaff[a], J. Ottarson[a], J. Wang[a], F. Deák[b], Á. Horváth[b], Á. Kiss[b], Z. Seres[c], K. Ieki[d], Y. Iwata[d], H. Schelin[e]

[a] National Superconducting Cyclotron Laboratory and Department of Physics and Astronomy, Michigan State University, East Lansing, MI 48824, USA
[b] Department of Atomic Physics, Eötvös University, Puskin utca 5-7, H-1088 Budapest 8, Hungary
[c] KFKI Research Institute for Particle and Nuclear Physics, 1525 Budapest 114 POB 49, Konkoly-These út 29-33, Hungary
[d] Department of Physics, Rikkyo University, 3 Nishi-Ikebukuro, Toshima, Tokyo 171, Japan
[e] Centro Federal de Educação Technologica, Av. Sete de Setembro 3165 80230-901, Curitiba, Pr, Brazil

Abstract

To further study neutron-rich halo nuclei, we have constructed a neutron detector array. The array consists of two separate banks of detectors, each of area $2 \times 2 \, m^2$ and containing 250 l of liquid scintillator. Each bank is position-sensitive to better than 10 cm. For neutron time-of-flight measurements, the time resolution of the detector has been demonstrated to be about 1 ns. By using the scintillator NE-213, we are able to distinguish between neutron and γ-ray signals above 1 MeV electron equivalent energy. Although the detector array was constructed for a particular experiment it has also been used in a number of other experiments.

PACS: 29.40.Mc; 29.30.Hs
Keywords: Neutrons; Time of flight

1. Motivation

We have constructed at the National Superconducting Cyclotron Laboratory (NSCL) the *Neutron Wall Array*, a large-area, position-sensitive neutron detector with neutron/γ-ray discrimination capabilities. First, we discuss the original motivation

behind the construction of the Neutron Wall Array and the original design requirements. Next, we present an outline of the physical construction and demonstrate some of the primary functions of the detector. We then present some of the operational procedures that have been used in experiments to date.

1.1. Radioactive nuclear beam advances

Our original motivation for building the Neutron Wall Array was to improve and extend

* Correspondence address: Deloitte & Touche Consulting Group, Two World Financial Center, New York, NY 10281-1420, USA. Tel.: +1 212 436 6149; fax: +1 212 436 5957; e-mail: pzecher@dttus.com.

measurements made at the NSCL of neutron-rich nuclei. These measurements are part of an extensive research program the NSCL has developed around its production of radioactive nuclear beams (RNBs). One of the biggest opportunities RNBs offer is the chance to study systematically isotopes far from the limits of stability. Many of these unstable isotopes are very neutron rich, and neutron detection has played an important roll in probing their structure. The nature of RNBs has also led to a change in the size and scope of the neutron detectors that are needed.

The primary difference in working with RNBs is a great reduction in intensity compared to beams of stable nuclei. RNBs are produced by sifting through the many fragmentation products created when an intense primary beam of heavy-ions strikes a target. As the product of a nuclear reaction, an RNB intensity is much lower than a primary beam intensity. A typical experiment with a stable beam would have an intensity of about 10^{12} particles per second; in contrast, an experiment with an RNB might have an intensity of 10^2–10^3/s. With such low intensities, it is desirable to cover as much solid angle as possible to reduce the beam time necessary to acquire sufficient statistics for an experiment.

The reduction in beam intensity is even more acute if two or more neutrons must be detected in coincidence. Unlike most charged-particle detectors, neutron detectors do not have 100% efficiency. A common value for one-neutron detection efficiency is about 10%. If two neutrons are to be detected in coincidence, then the combined efficiency falls to 1%. Since the two-neutron detection efficiency goes as the square of the one-neutron efficiency, it is advantageous to try to increase the one-neutron efficiency.

1.2. The $^{11}Li(\gamma,2n)^9Li$ experiment

One of the early clues to the richness of RNBs was the anomalously large cross section for ^{11}Li interacting with various target nuclei [1]. For years, the nuclear density was thought to be nearly constant throughout the table of isotopes, but studying ^{11}Li has demonstrated that far from stability, the valence nucleons may form a low-density halo around a more normal core. A recent experimental study of ^{11}Li [2–4] is an excellent example of the added complexities of working with neutrons from RNB experiments. First, the experiment required two neutrons to be detected in coincidence, and second, the available beam intensity was only 500 ^{11}Li per second. The Neutron Wall Array was constructed to replace the neutron detectors used in this experiment with a device that has better resolution and efficiency. What follows is a brief description of this experiment and the limitations of the neutron detectors used.

In 1991, Sackett et al. [2] performed an experiment to measure the soft-dipole-resonance parameters and ground-state n–n correlations of ^{11}Li [2–4]. To accomplish this, they made a kinematically complete measurement of the coulomb dissociation of ^{11}Li as it passed through the virtual photon field of a Pb nucleus. In this situation, if the ^{11}Li absorbed a virtual γ-ray from the Pb nucleus, it could dissociate into a ^{9}Li and two neutrons. By measuring the velocities of the ^{9}Li fragment and the neutrons, it was possible to determine the γ-ray energy for each event and then determine the $(\gamma, 2n)$ excitation function from the collection of events.

The experimental setup they used is shown in Fig. 1. A beam of 30 MeV/nucleon ^{11}Li projectiles was incident on a Pb target after passing through two position-sensitive parallel-plate avalanche counters (PPACs) used to determine the incident path of each ^{11}Li. After dissociation in the Pb target, the ^{9}Li fragment energy and position were measured in a Si–CsI telescope about 15 cm downstream from the target. The two neutrons passed through the telescope and were detected in two arrays consisting of 54 small scintillation detectors. The arrays were placed 5 and 6 m downstream and subtended a maximum half-angle of 5°. Each neutron's energy was determined by measuring its time of flight from the target. The neutron's direction was determined by knowing which detector it hit.

The neutron detectors used were small cylindrical scintillation counters of the type shown in Fig. 2. The liquid scintillator was housed in an aluminium can; one end of the can was open and optically coupled to a large plastic light pipe attached to a photomultiplier tube. The neutrons were incident parallel to the axis of the cylinder.
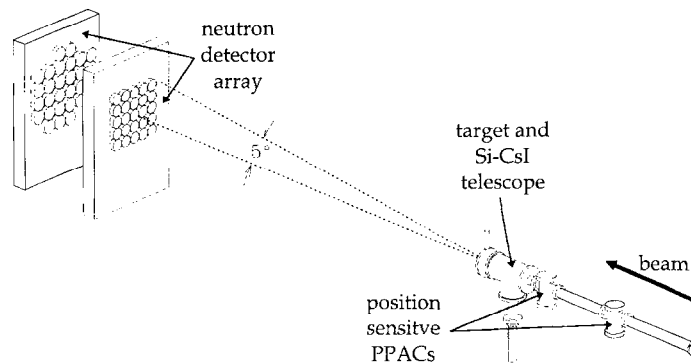
Fig. 1. Experimental setup to measure the complete kinematics of ^{11}Li → ^{9}Li + 2n events [2].
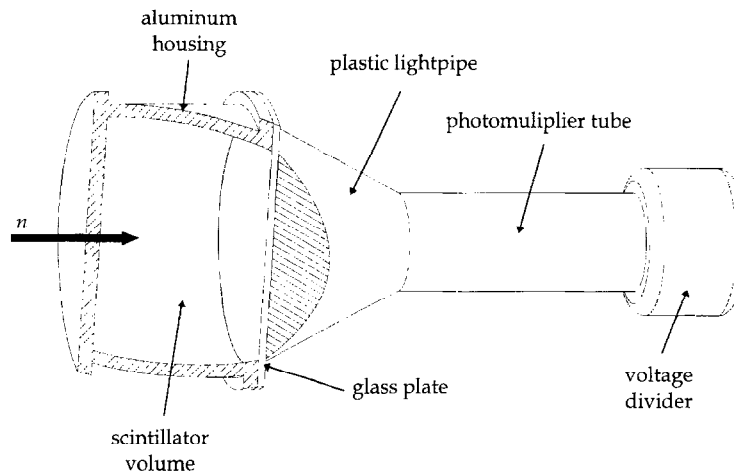

Fig. 2. A cutaway diagram of a neutron detector used by Sackett et al. [2]. Neutrons are incident from the left. The scintillator is 12.7 cm in diameter and 6.7 cm deep for a volume of 0.97 l.

When these detectors are stacked in a tight array, the cylindrical design creates a minimum 50% dead space between the detectors, decreasing the array's efficiency. To help boost the efficiency, a second array was added behind the first. Unfortunately, adding the second array also complicates the analysis by enhancing the effects of cross-talk and out-scattering.

Cross-talk is the familiar problem of one neutron creating signals in two separate detectors. In out-scattering a neutron scatters from the non-active part of a detector and is then detected in a different

detector with incorrect position and time of flight (TOF) and, therefore, energy values. While methods exist for identifying and eliminating cross-talk events from the data, there are no methods available for identifying out-scattered events. Therefore, the neutrons should pass through as little non-active material as possible. Unfortunately, the neutron detectors used in the array had a ratio of total mass to active mass of over 4 to 1.

For small decay energies, the reaction products were forward-focused, and the setup provided satisfactory solid angle. Given a one-neutron detection

efficiency $\varepsilon_{neutron}$ of 10% for each detector in the array and the factor 1/2 for the empty space in the array, a ^{11}Li reaction probability in the target $P_{reaction}$ of 1%, and a beam intensity I of 500 ^{11}Li/s, a simple estimate of the counting rate is

$$\varepsilon_{neutron}\varepsilon_{neutron}P_{reaction}I$$

$$= (0.1 \times \tfrac{1}{2})(0.1 \times \tfrac{1}{2})(0.01)(500) = 0.0125 \text{ events/s}.$$

For larger decay energies, the counting rate drops as the solid angle drops.

The success of Sackett's experiment and the intense interest in neutron-rich nuclei has led us to attempt to improve the experiment. To overcome many of the limitations imposed on Sackett's experiment by the neutron detector array, we proposed, designed, and constructed the Neutron Wall Array. We had four main objectives when designing the Neutron Wall Array:

(1) increase the angular acceptance of the array by increasing its area;

(2) greatly decrease the dead space between the individual detectors;

(3) reduce the inactive (non-scintillator) mass through which the neutrons must pass to reduce out-scattering;

(4) while increasing the area (1 above) decrease the ratio of the number of electronic channels to the scintillator volume.

This last point is simply one of cost savings; as an example, if we duplicated the existing detectors to cover the same solid angle as we cover with the new detector, we would need over 500 individual detectors, each with its own channel of associated electronics. The Neutron Wall Array has 100 channels.

To meet our objectives, we used the well-known geometry of long rectangular scintillator cells, placed perpendicularly to the beam axis. Each cell is viewed at both ends by photomultiplier tubes (PMTs). With 25 cells, each 2 m long, we cover an area of 4 m^2 in each wall. Using the same flight path as in the previous experiment, the array subtends a half-angle of 15°, whereas the previous array only subtended a half-angle of 5°. A time signal for the TOF measurement is obtained from the mean time of the PMT signals. The position of the event along the cell is determined from the time difference

between the signals. The thickness of the cell in the beam direction is limited by the energy resolution we wish to achieve.

Complicating the detector's design is the requirement that the detector be capable of pulse-shape discrimination (PSD) in order to distinguish between neutron and γ-ray events. When the TOF method is used to determine energy, a time-independent γ-ray background introduces a continuous background in the neutron energy spectrum. We wish to study a continuous neutron energy spectrum, so we must have some method of removing this γ-ray background from the neutron spectrum. Also, γ-ray identification plays an important role in cross-talk rejection. The complication in the design arises because the only scintillators capable of PSD are a few liquid hydrocarbon scintillators. Instead of the self-supporting plastic bars of scintillator that are usually employed, our scintillator is housed in long, cast Pyrex tubes that are sealed at both ends. Although the Pyrex cell adds non-active material through which neutrons must pass, the ratio of total mass to active mass is much less than with the previous detector configuration.

2. Neutron Wall Array characteristics

The Neutron Wall Array consists of two walls, each with 25 detector cells. The area of each wall is 2×2 m^2; the inactive area is less than 12% of the total area – much less than the 50% in Sackett's [2] array. The scintillator used is NE America's NE-213 and the total scintillator volume is 500 l. Currently, the Neutron Wall Array resides in the NSCLs N4 vault (see Fig. 3) and has access to beams from the A1200 Spectrograph. The overall time resolution of the array is about 1 ns FWHM with a corresponding position resolution along the length of the cell of 7.7 cm FWHM. This position resolution is comparable to the 7.62 cm height of the individual detector cells. We have obtained excellent PSD for neutrons with energies above 3 MeV.

By placing two arrays back to back, we can obtain a detection efficiency of about 20% for the detectors, with only 12% empty space. Using these values, the counting rate in Sackett's experiment
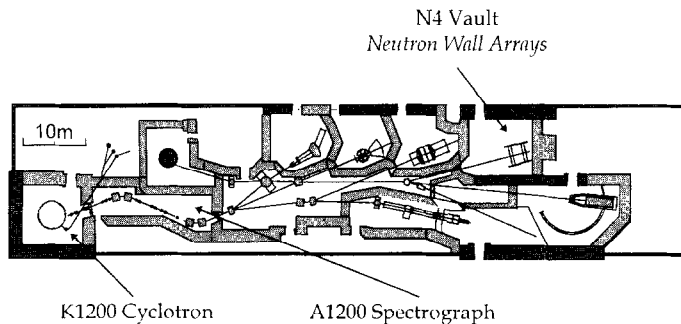
N4 Vault
Neutron Wall Arrays

Fig. 3. The NSCL experimental areas.

would be

$$\varepsilon_{neutron}\varepsilon_{neutron}P_{reaction}I$$

$$= (0.2 \times 0.88)(0.2 \times 0.88)(0.01)(500)$$

$$= 0.155 \text{ events/s.}$$

By increasing the solid angle from a half-angle of $5°$ to $15°$, we have increased to 1 MeV the decay energy for which the geometric efficiency is 100%.

Given the general operating parameters of the NSCLs cyclotron, neutrons from nuclear reactions can have energies up to a few hundred MeV. The neutron's lack of charge makes it very difficult to detect directly. Therefore, almost all methods of detecting neutrons in this energy range involve imparting some or all of the neutron's kinetic energy to a charged nucleus that is then detected. The simplest means of doing this is to transfer some of the neutron's energy through elastic scattering, creating a recoil nucleus. Since the energy of a recoil nucleus will be a random fraction of the neutron's energy, we cannot determine the neutron's energy by measuring the energy of the recoil nucleus. To determine the neutron's energy, we measure the time the neutron takes to travel from the target to the detector. Then, if the length of the flight path is known, we can determine the neutron's velocity and energy, regardless of the energy deposited in the detector.

The more energy the recoil nucleus has, the easier it is to detect. Simple two-body kinematics show that the maximum recoil energy is achieved when the recoil nucleus has the same mass as the neutron. Therefore, it is preferable to use hydrogen as the

primary scattering target for neutron detection. Detectors based on hydrogen scattering are called *proton recoil detectors.*

Scintillation detectors are among the most popular devices used as proton recoil detectors. Scintillation detectors convert the kinetic energy of ionizing radiation into detectable light pulses. In the case of neutron detection, the ionizing radiation is an elastically scattered recoil proton from a hydrogen atom in the scintillator material. Most recoil protons will deposit all of their energy in the scintillator since the range of the recoil proton is typically much less than the dimensions of the detector. Although many materials are available as scintillation detectors, the most commonly used materials are organic solvents and plastics that contain an organic scintillant.

Section 2.1 describes the general physical characteristics of the Neutron Wall Array; Section 2.2 briefly describes the measured time resolution of the array; Section 2.3 discusses measurements of the position resolution along the length of a cell; and Section 2.4 demonstrates the PSD properties of a cell.

2.1. Size, configuration and construction

The elements that form the array are 2 m long Pyrex cells filled with the liquid, organic scintillator NE-213. Two PMTs view the cell from both ends. Fig. 4 shows a drawing of one cell. The outside of the Pyrex cell is not treated with any reflective or specular coating. This allows total internal reflection to be the means by which the light is
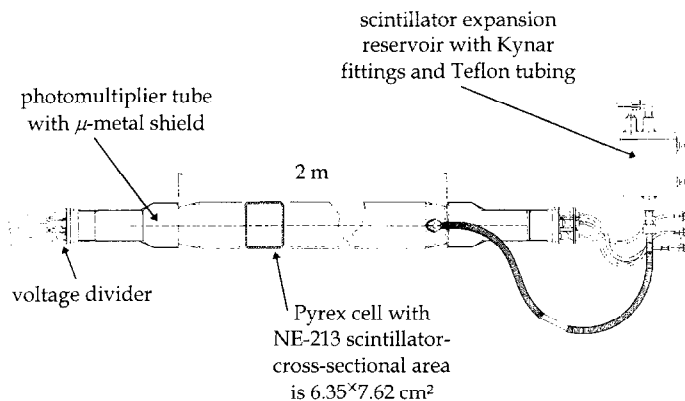
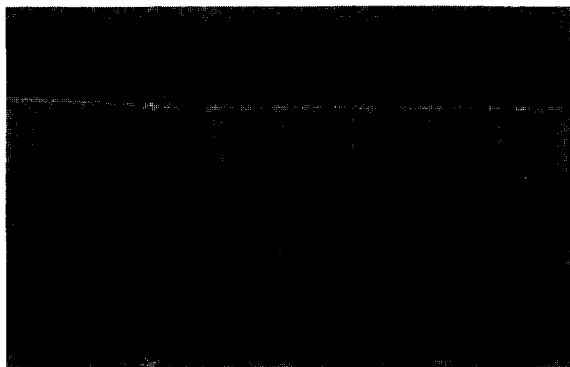Fig. 4. Drawing of an individual detector cell from the Neutron Wall Array.

Fig. 5. Photograph looking lengthwise through a cell. The NSCL logo was placed at the opposite end of the cell. All but the center image result from total internal reflections from the sides of the cell.

channeled through the cell to the PMTs. Monte Carlo simulations of the detector show that approximately 20% of the light from an event reaches each PMT; the other 60% of the light escapes from the cell because the angle it forms with the surface normal of the glass is less than the critical angle. Fig. 5 is a photograph taken through one end of a cell; the NSCL logo was placed at the other end. Multiple reflections of the logo in the sides of the detector are visible. (The cell used for the photograph had a square cross section and was not one of the cells used in the Neutron Wall Array, which have a rectangular cross section.)

The Pyrex cells were custom-made for this application and have a wall thickness of 3 mm. To make the cell, we purchased Pyrex tubing made to our cross-sectional specifications, at least 2.1 m long, and with ends open. The Michigan State University Scientific Glass Blowing Shop then closed the ends of the tubes so that they could be coupled to the PMTs. The PMT used was a new product of Philips Photonics, model XP4312B/04. This model is a fast, 12-stage PMT with a 7.5 cm photocathode surface. In order to make use of the whole photocathode surface, the ends of the tubing were closed off with 7.5 cm circular Pyrex disks. Closing an end was a two-step process. First, a Pyrex cylinder 7.5 cm in diameter was fused onto the end of the rectangular tubing. The cylinder was then trimmed at the nearest point to the junction where the cross-section became circular, about 3 cm. The second step was to fuse a circular plate 7.5 cm in diameter onto the cylinder. Except for cleaning, the surfaces of the cells required no further polishing or finishing and were used as they came from the manufacturer.

Before a cell was sealed, a tube, 6 mm in diameter with a glass-Kovar seal, was fused onto the cell. The tube is connected to an aluminium can by a corrugated Teflon tube. This can allows for thermal expansion of the scintillator, since the scintillator's coefficient of expansion is greater than the glass's. The scintillator will corrode most plastics; therefore, all of the tubing and fittings are made of Teflon or Kynar, both being chemically resistant to

the scintillator. Once the can was in place, some long, narrow (3 mm OD) Teflon tubing was inserted through the can and corrugated Teflon tube into the cell (see Fig. 6). The scintillator was then pumped through the narrow tubing, filling the cell.

The PSD properties of NE-213 can be degraded by the presence of dissolved oxygen in the scintillator. To remove any oxygen that might have been introduced when the cell was filled, we passed dry nitrogen gas throughout the volume of the scintillator for about 1 h. The nitrogen gas was delivered into the cell through the same Teflon tubing that was used to fill the cell. When this process was complete, the Teflon tube was removed and the aluminum can was sealed with a stainless-steel pipe plug.
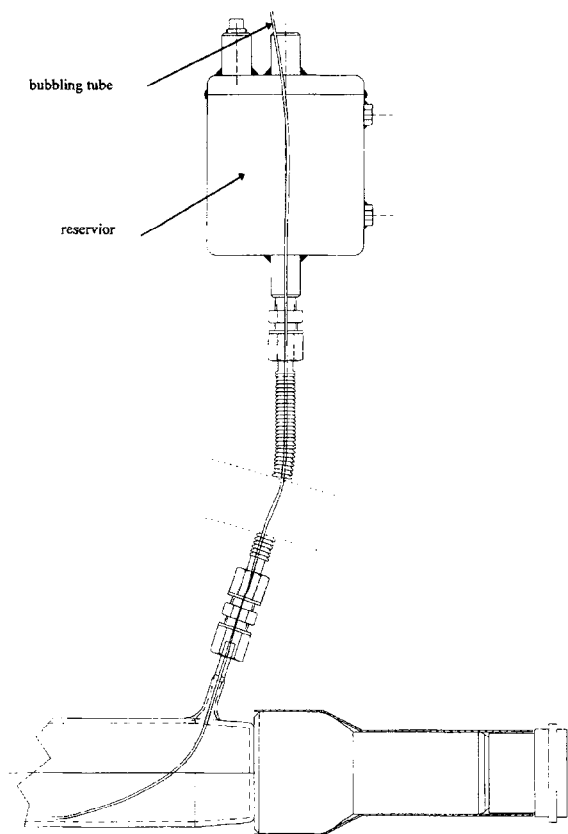

Fig. 6. Schematic drawing of the bubbling setup for a completed cell. For about 1 h, dry nitrogen gas is blown through the narrow Teflon tubing that is fed through the reservoir into the cell.

Before a cell was filled, the PMTs were attached to its ends with the optically clear epoxy BC-600. A special jig was designed to hold the PMT and cell in place for the 24 h the epoxy requires to cure. Surrounding each PMT is a μ-metal shield; this prevents any extraneous magnetic fields from interfering with the operation of the PMT. We designed a simple passive voltage divider for our PMTs. Both the anode and last dynode signals are used by the acquisition electronics. Fig. 7 shows the voltage-divider circuit. The total resistance of the resistor chain was selected to use the maximum current available from the power supply. Having a large current flow through the resistor chain helps maintain the linearity of the signal amplification.

After the cells were completed, they were mounted on two aluminum frames. In case of a catastrophic accident, the bottom of each frame has a catch-basin capable of containing the scintillator volume from all 25 cells in the frame. The sides and top of the frame are covered with aluminum plates and made light-tight with opaque caulking. The front and back of the frame are covered with a removable aluminum sheet attached at the edges to another aluminum frame. The aluminum sheet is 0.8 mm thick, providing very little material for unwanted neutron scattering. A cutaway drawing of the complete assembly is shown in Fig. 8.

The cells were attached with brackets to two, hollow, 5 cm square aluminum posts in the center of the frame. The cells were strapped to the bracket with 0.5 mm thick stainless-steel bands (see Fig. 9). To allow for small variations in the surface of the cell, the cells are spaced 3 mm apart. Once a cell was in place, the aluminum can was opened and attached to a nitrogen gas manifold to provide a greater gas volume for expansion.

The inside of each of the aluminum frames is painted flat black, and when the front and back cover sheets are in place, the aluminum box becomes light tight. By making the frame light tight, we have avoided the difficulty of making the 50 cells light-tight individually. To prevent optical cross-talk between the cells – i.e., light from one cell entering a neighboring cell – a long strip of black paper was placed on the top of each cell.

Other miscellaneous hardware associated with the two frames include a gas-monitoring system, an

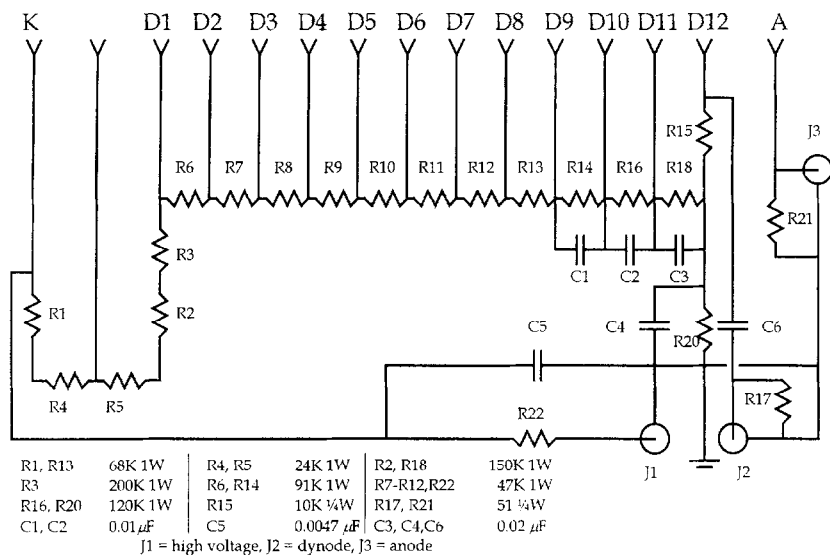| R1, R13 | 68K 1W | R4, R5 | 24K 1W | R2, R18 | 150K 1W |
R3	200K 1W	R6, R14	91K 1W	R7-R12,R22	47K 1W
R16, R20	120K 1W	R15	10K ¼W	R17, R21	51 ¼W
C1, C2	0.01 μF	C5	0.0047 μF	C3, C4,C6	0.02 μF

J1 = high voltage, J2 = dynode, J3 = anode

Fig. 7. Schematic drawing of the passive voltage divider used on the Philips XP4312/04 PMT.
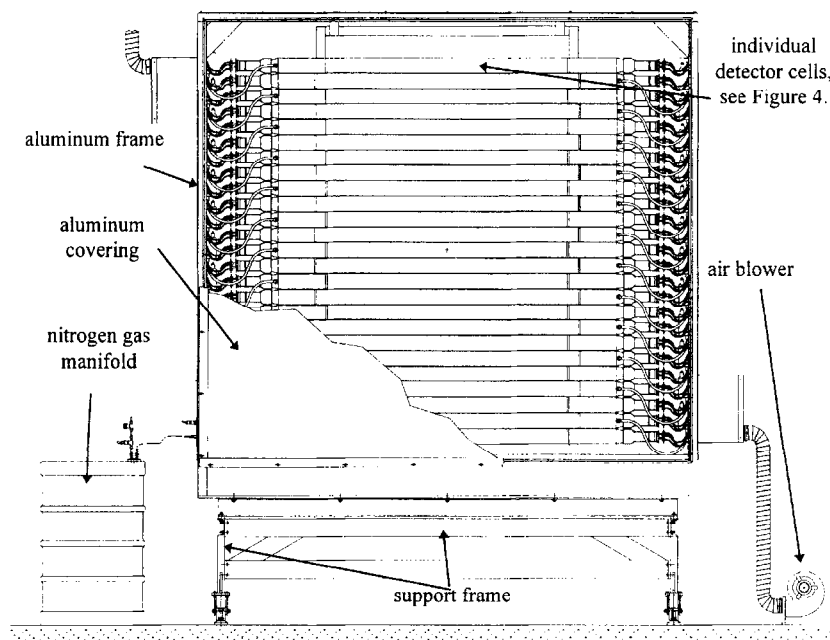
Fig. 8. Mechanical cutaway drawing of one wall of the Neutron Wall Array.

air blower, and a fiber-optic timing system. The gas monitor detects high levels of xylene, which is the solvent for the scintillator. This gas is explosive and the liquid has a flash point of 36°C. The gas moni- tor is connected to the laboratoy's electronic con- trol system. If the gas monitor detects a dangerous level of xylene, it alerts the control system, which shuts down the high-voltage system powering the
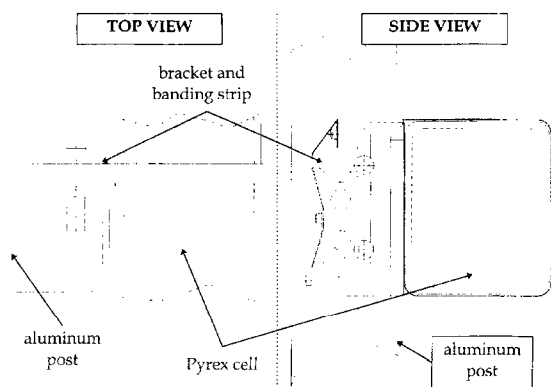
Fig. 9. Top and side view of the cell-mounting bracket.

PMTs. Each of the voltage dividers produces 5 W of heat. To help keep the inside of the frame cool, each frame has an air blower. To keep the frames light-tight, the blowers are connected to the frames through light-tight baffles. The fiber-optic system is used for various timing purposes and is discussed in Section 3.2.2.

Each of the two walls is supported on a steel frame that centers the wall about the beam height in the N4 vault, where the Neutron Wall Array is used. The steel frames are on wheels and can be moved independently about the vault. The frames are also designed to nest into each other so that the arrays can be placed front to back, if the user so desires, with a minimum distance between the cells of about 30 cm.

2.2. Time-of-flight energy resolution

Determining a neutron's energy by measuring the time a neutron takes to travel a known distance is called the time-of-flight (TOF) method. Three factors that contribute to the time resolution are the rise time of the light pulse in the scintillator, the intrinsic time resolution of the electronics, and the intensity of the scintillation light. These three factors are characteristics of the scintillator and electronic equipment available. Other factors affecting the time resolution are the collection efficiency of the available light and the thickness of the scintillator. These last two factors are geometric properties of the detector's design.

The light pulse arrives at the PMT as a series of photons spread out over some time interval. The electronics used to time the neutron requires a logic pulse that is generated when a sufficient number of photons has arrived at the PMT to surpass some threshold. (The threshold could be one photon, but the quantum efficiency of the photocathode surface is not unity, so the time pulse might not correspond to the first photon that arrives at the photocathode surface.) Therefore, the time of the logic pulse relative to the actual scintillation event can vary depending on the statistics associated with the number of photons required to trigger the logic pulse. A more luminous pulse will create a higher density of photons per unit time, thus improving the time resolution.

In organic liquid and plastic scintillators light is emitted isotropically. Since the number of photons going straight to a PMT drops off as $1/r^2$, most of the light collected by the PMT will have scattered from one or more sides of the cell before reaching it. This variation puts an uncertainty into the photon's flight path and flight time and can, therefore, add to the uncertainty in the true start time of the scintillation pulse.

The final contribution to a detector's time resolution comes from the finite time it takes a neutron to pass through the detector. Fig. 10 shows a schematic diagram of our rectangular scintillator detector some distance from a neutron source. The scintillator is viewed at both ends by PMTs. As a neutron penetrates the scintillator, it has a uniform
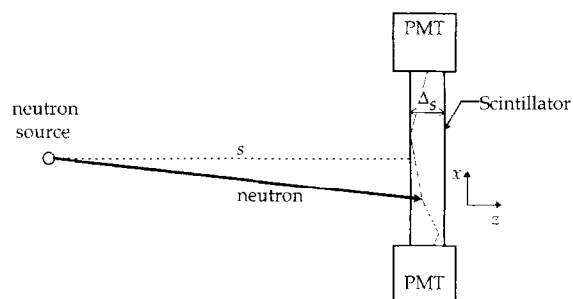

Fig. 10. Schematic drawing of a neutron being detected in a long scintillator cell. Two photon paths are shown, one going to each PMT and both originating at the point of neutron interaction. To show these details, the cell thickness Δs has been magnified by a factor of 5.

scattering probability as a function of depth. Since the PMTs are unable to locate the position of the scintillation in the z-direction, there is an uncertainty Δs in the distance s from the source to the scattering event. It is useful to express this uncertainty in terms of a time uncertainty, $\Delta t = t\Delta s/s$, related by the neutron's velocity, $v = s/t$. Then, for a given thickness of detector, the time resolution depends on the flight time of the neutron through the scintillator, and therefore on the neutron's energy.

Increasing the cell's thickness worsens the detector's time resolution, but it increases its efficiency. The thickness chosen is therefore a compromise between the desired efficiency and the desired energy resolution. It is often best to choose a thickness that creates a Δt comparable to the other time resolution characteristics.

If the neutron's energy is determined by its TOF over a flight path s,

$$E = \frac{1}{2}n\left(\frac{s}{t}\right)^2,$$ (1)

and there are uncertainties σ_s in the flight path and σ_t in the time, then the uncertainty in the neutron's energy is

$$\sigma_E^2 = \sigma_s^2\left(\frac{\partial E}{\partial s}\right)^2 + \sigma_t^2\left(\frac{\partial E}{\partial t}\right)^2.$$ (2)

Or, expressed as the relative energy resolution,

$$\frac{\sigma_E^2}{E^2} = 4\left(\frac{\sigma_s^2}{s^2} + \frac{\sigma_t^2}{t^2}\right).$$ (3)

It is often difficult to determine the overall time uncertainty σ_t from each of the contributions discussed. Luckily, there is a process by which the overall σ_t can be determined. When a TOF spectrum is observed for neutrons from a nuclear reaction, there is also present a distinct, narrow peak associated with the prompt γ-rays from the reaction. Since the γ-rays all move at the speed of light, their transit time through a thin scintillator detector is considerably less than the neutron's transit time. The width of the γ-ray peak, thus, represents the time uncertainty for the whole system with only a small contribution from detector thickness. (The γ-ray's emission time does not contribute to the

uncertainty, since the γ-rays are emitted on the time scale of electromagnetic nuclear transitions, very much less than typical laboratory resolution of ~ 1 ns.) Using the width of this γ-ray peak and the detector thickness, we can determine the relative energy resolution σ_E/E.

Fig. 11 [5] shows a typical time-of-flight spectrum from the Neutron Wall Array. The γ-ray peak is clearly visible at the right edge of the spectrum. The FWHM of this γ-ray peak is about 1 ns.

2.3. Position sensitivity

The x-position of an event in the cell is determined from the time difference between the two PMT signals. The position resolution is therefore related to the time resolution of the system by a time-to-distance calibration. To obtain this calibration, it is necessary to position a collimated source at different locations and measure the time differences. This value cannot be calculated from the speed of light in the scintillator because the time signal from the PMT is not based on direct light from the source. Rather, the time signal is mostly the result of light that scatters from the sides of the cell before reaching the PMT.
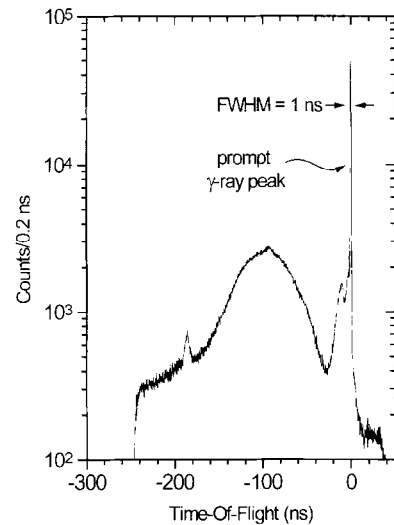

Fig. 11. Neutron and γ-ray TOF spectrum from Ar on Ho at 25 MeV/nucleon. The prompt γ-ray peak from the reaction is an indication of the overall time resolution of the Neutron Wall Array [5].
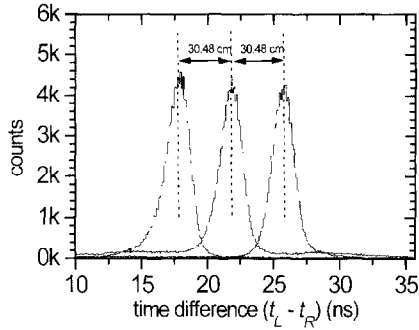
Fig. 12. Time difference measurement of a collimated ⁶⁰Co source at three different positions. The positions are separated by 30.48 cm.

Fig. 12 shows three different collimated source measurements as a function of time difference (with an arbitrary offset). Each peak is 30.48 cm from its neighbor, giving a distance-to-time calibration of 7.65 cm/ns. The time resolution shown in the previous section is about 1 ns; therefore, the position resolution approaches 7.65 cm for high-energy events.

2.4. Pulse-shape discrimination

Proton recoil scintillation detectors are sensitive to more than just neutrons. Typically, a large background of γ-rays and cosmic-rays is present during an experiment. A few possible methods exist for managing these background radiations.

The most useful method of reducing background events comes from analyzing the electric pulse from the PMT. For some scintillators, the shape of the pulse varies according to the specific ionization of the ionizing particle. The light produced by an ionizing particle has two components, a prompt fluorescence and a delayed fluorescence. The prompt fluorescence has a decay constant of a few nanoseconds, whereas the delayed fluorescence has a decay constant on the order of a few hundred nanoseconds. The proportion of light produced by each of these two components varies according to the specific ionization of the ionizing particle. A lightly ionizing particle, such as a cosmic-ray muon or an electron from the compton scattering of a γ-ray, will produce a small fraction of its light

in delayed fluorescence. A more highly ionizing particle, such as a recoil proton from neutron scattering, will produce a larger fraction of its light in delayed fluorescence. Hence, the time shape of the pulse for neutrons is different from what it is for background γ-rays and muons.

Over the years, many procedures have been developed to exploit this PSD property. Most methods are able to discriminate between γ-ray and neutron signals for neutron energies above 3 MeV. A method developed at the NSCL [6] uses two ADCs: one integrates the total charge of the pulse, and the other integrates the charge for some fixed time fraction of the pulse. The fixed time fraction is usually either the head of the pulse or the tail of the pulse. By comparing the charge in this fraction of the pulse to the total charge in the pulse, we can determine which species of particle created the pulse.

Most PSD methods are not suitable to a detector as large as the Neutron Wall Array. To overcome their difficulties, we developed a new method which will be published separately. Our method produces a signal called QFAST, which is proportional to the charge in the head of a pulse from a PMT. If QTOTAL is the total integrated charge from a PMT, then for a given value of QTOTAL, the value of QFAST is different for γ-rays and for neutrons.

Both QFAST and QTOTAL are dependent on the distance of the event from the PMT because the light is attenuated by the scintillator. To compensate for this, we create position-independent QFAST and QTOTAL signals by taking for each the square root of the product of the QFAST and QTOTAL signals from the two PMTs. If the light has a $1/e$ attenuation length of λ (~ 1.5 m in NE213), then the luminosity at one of the PMTs is $L_{PMT} = L_0 e^{-x/\lambda}$, where L_0 is the initial luminosity and x the distance to the PMT. If the other PMT is a distance l (the length of the cell) away from the first PMT, then its luminosity is $L_{PMT2} = L_0 e^{-(l-x)/\lambda}$. Taking the square root of the product of these two measured luminosities we obtain

$$L_{measured} = \sqrt{L_{PMT}L_{PMT2}} = L_0 e^{-l/\lambda}, \qquad (4)$$

where $L_{measured}$ is independent of the position of the event within the cell. Not only do we use $L_{measured}$ for the PSD, we also use $L_{measured}$ to set a lower-limit threshold in the software. Since this

threshold is insensitive to the position of the event, the efficiency is uniform along the cell. For the rest of this section, QFAST and QTOTAL refer to the position-independent values.

In Fig. 13 we show QFAST plotted against QTOTAL. Since QTOTAL is proportional to the light output, it can be related to either the compton scattered electron energy or the recoil proton energy. It is easier to represent QTOTAL in terms of the electron-equivalent energy than in terms of the recoil proton energy since, unlike the proton, the electron's light output is linearly dependent on its energy and the proton's light output is not linear.

Fig. 14 shows QFAST for various values of QTOTAL, which is again represented in terms of electron-equivalent energy. It is clear from the figure that we have achieved excellent neutron/γ-ray discrimination to below 1 MeV electron-equivalent energy, or a recoil proton energy of about 3 MeV. To quantitatively discuss the PSD property of a scintillator, we calculate the so-called figure of merit (FOM). The FOM for one of the spectra in Fig. 14 is defined as the separation between the two centroids of the peaks divided by the sum of the FWHMs of the two peaks. We consider a FOM above 1.0 to be acceptable. By fitting a double Gaussian to the data in Fig. 14 we determine the FOM shown in Fig. 15 as a function of electron-equivalent energy.
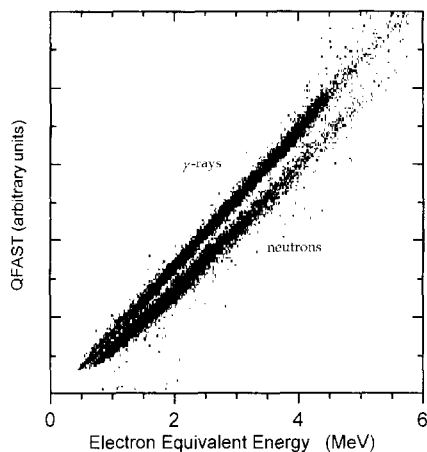
3. Operation

The following sections deal with various aspects of operating the Neutron Wall Array. Of primary interest is the electronics system used to obtain the necessary information from the cells in the array.
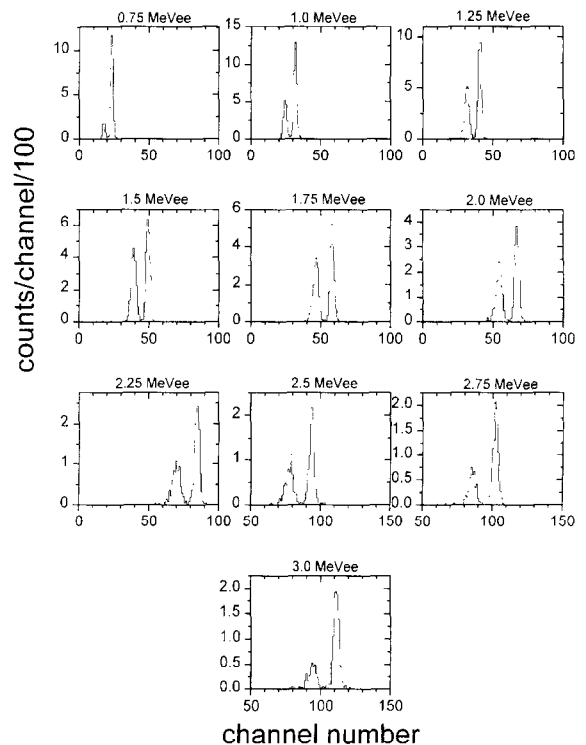

Fig. 14. Individual QFAST spectra for various QTOTAL values. The QTOTAL values are expressed in terms of electron equivalent energy.

Fig. 13. A PSD spectrum from a cell in the Neutron Wall Array. The neutrons and γ-rays are from a Pu–Be source placed 1 m perpendicularly from the center of the cell.
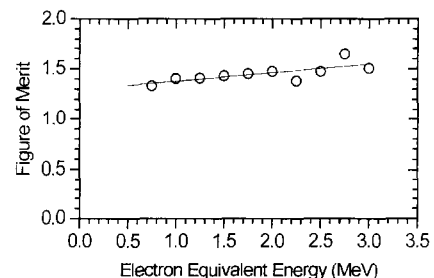

Fig. 15. Figure of merit from Fig. 14 as a function of the light intensity in units of electron equivalent energy.

Also of interest are the two primary calibrations that must be performed when the Neutron Wall Array is used.

3.1. Electronics

For every event in the Neutron Wall Array we must know the time of the event with respect to some reference signal (e.g., the time of a fragment event or of the cyclotron RF), the position of the event along the cell, and the energy of the recoil proton. We must also record QFAST and QTOTAL to do PSD.

By measuring the time between some reference signal and each of the PMTs on a cell, we can find both the time of the event and the position of the event along the cell. If t_L is the time between the reference signal and the left PMT, and t_R is the time between the reference signal and the right PMT, then to first order, the time of flight of the event is

$$TOF = \frac{t_L + t_R}{2}, \tag{5}$$

and the position from the center of the cell is

$$position = k(t_L - t_R), \tag{6}$$

where k is the scale factor between time and distance (see Section 2.3). Higher-order terms would correct for non-linear effects at the extreme ends of the cell.

We determine the energy of the recoil proton from QTOTAL (see Section 3.2.1). If there is a large dynamic range in the recoil proton energies, we must also produce attenuated versions of QFAST and QTOTAL.

Fig. 16 shows a simple schematic of the electronics used to obtain this information from a PMT. All of the information is obtained from the two electrical signals produced by the PMTs voltage divider. One signal is a positive-voltage pulse from the last dynode in the multiplier chain and the other signal is a negative-voltage pulse from the anode that collects the charge from the multiplier chain. The dynode pulse is used for the timing signal, and the anode pulse is used for the integrated charge signals. Most timing electronics use negative pulses, so we invert the dynode pulse with
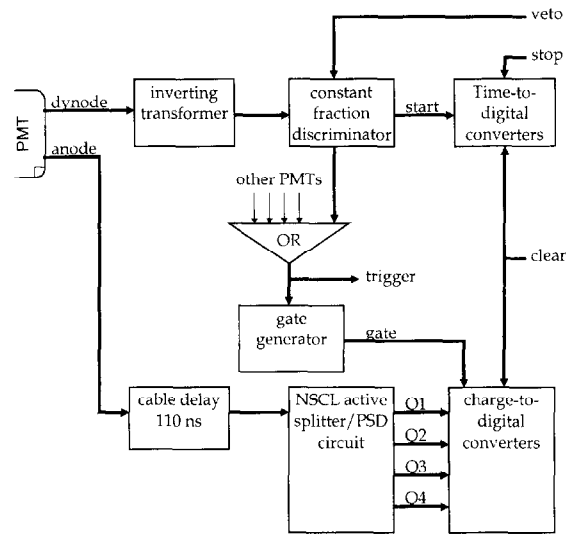

Fig. 16. Basic outline of the processing of the signals from the Neutron Wall Array. Q1–Q4 represent the charge signals: anode, attenuated anode, PSD, and attenuated PSD.

a small inductor. This inverted signal is fed into a constant fraction discriminator (CFD). The CFD produces a fast logic pulse if the voltage of the input signal surpasses a programmable threshold. The logic output of the CFD is then used to start a fast clock, a time-to-digital converter (TDC). The clock is stopped by the common reference signal. A logical OR of all of the CFD outputs is used to create a gate signal, which controls the charge-to-digital converters (QDCs), and a trigger signal for the primary trigger logic which controls the data acquisition computer.

Our traditional method of doing PSD [6] is shown in the upper part of Fig. 17. The anode signal is split and fed into two QDCs. One of the two signals is delayed 30 ns before being fed into the QDC. A gate signal is then timed so that it begins with the start of the delayed signal; the QDC integrates the pulse as long as there is a gate signal. While this method works very well, it is not suited for applications where two (or more) neutrons must be detected in coincidence. The problem is, if two neutrons arrive at different times, two different gates are required. Unfortunately, most QDC modules have multiple channels controlled by one common gate. A few solutions exist. One solution is to
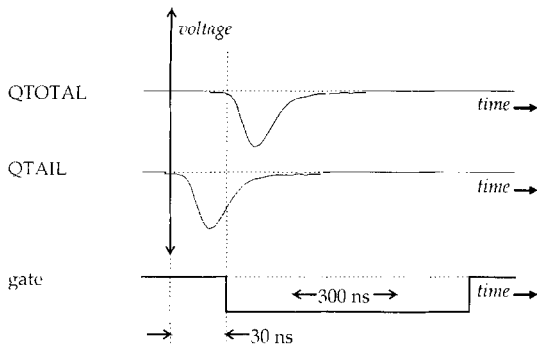
Fig. 17. Signals and gate used in pulse-shape discrimination [6].

Fig. 18. Primary trigger logic.

use one QDC module per PMT and only use two channels per module. The high cost of QDC modules makes this solution impractical if a large number of PMTs is involved. Another solution is to use a linear gate module as the input to the QDC, in effect giving each QDC channel its own gate. We prefer not to use this method because of insufficient stability of available linear gates. (This was the method used by Sackett et al. [2].)

While investigating other PSD methods, a suggestion arose for a very simple circuit that would create QFAST. The method of creating this pulse will be described in a separate publication. This pulse can be created any time during the gate period. With this method, we again split the anode pulse into two separate pulses. One of the two pulses is integrated to produce QTOTAL. As long as the gate starts before the pulse and lasts for approximately 300 ns after the beginning of the pulse, the position of the anode pulse with respect to the gate is arbitrary. The other pulse is used to create QFAST. It too can fall at an arbitrary time within wide gate. Hence, QFAST and QTOTAL are created equally well for each neutron in a two-neutron event.

The same signal that produces the gate for the QDCs is also used as the Neutron Wall trigger for the primary trigger logic. The primary trigger logic's job is to coordinate the Neutron Wall electronics with the rest of the electronics required by the experiment. Typically, the logic is designed to look for a coincidence between the Neutron Wall trigger and a signal in another detector. If such
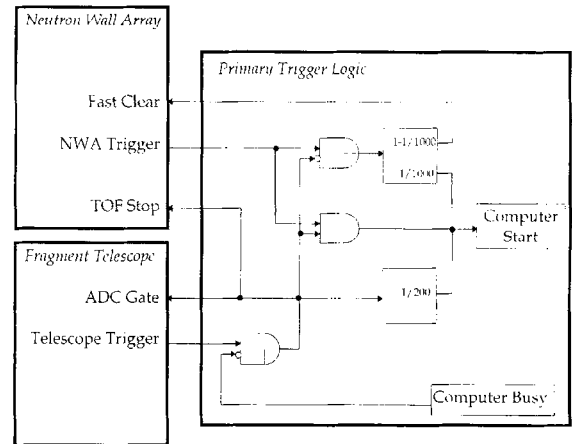
a coincidence is found, then the data acquisition computer is instructed to read the values of the QDCs and the TDCs. If the Neutron Wall triggers and there is no coincidence with the other detectors in the experiment, then the Neutron Wall electronics processes a fast clear. This resets all of the QDCs and TDCs. This is particularly useful because of the high background counting rate of the wall. With thresholds set to 1 MeV electron equivalent energy, the background counting rate is about 16000 events per second. By using the fast clear, these events are not processed by the data acquisition computer. This reduces the dead time of the system. Once the computer is activated, a veto signal is issued to all CFDs to prevent events from entering the electronics before the previous event is completely read out. A schematic drawing of the primary trigger logic that was used in the Neutron Wall's first experiment is shown in Fig. 18. To record some small fraction of the Neutron Wall events and fragment events that were not in coincidence, down-scaler units were used.

3.2. Calibrations

Two particular calibrations must be performed each time the neutron wall is used: a calibration of pulse height to energy, and a calibration of time per ADC channel. These calibrations are demonstrated below.

3.2.1. Pulse-height calibration

Although TOF is used to determine the neutron's energy, it is often useful to know the energy E_p of the recoil proton. The obvious method is to relate E_p to QTOTAL, and we explained in Section 2.4 (Eq. (4)) how a position-independent value can be made by taking the square root of the product of the two PMT pulse heights.

To calibrate the pulse-height spectrum we use various γ-ray sources. In the same manner that neutrons are detected through (n, p) scattering, γ-rays are detected through compton scattering. We use three different γ-ray sources for the pulse-height calibration: ^{60}Co, ^{228}Th, and ^{12}C ($E_x = 4.44$ MeV) in a PuBe source. Fig. 19 shows a sample pulse-height spectrum for each of the three sources. The energies shown are not the γ-ray energies, but the compton-edge energies of the recoil electron. The compton-edge energy is associated with the channel of the half-height value of the compton edge. Once the γ-ray calibration is known, we use an empirical expression relating equal amounts of light output from recoil protons of energy E_p (in MeV) and from recoil electrons of energy E_e (in MeV) [7]. The expression is

$$E_e = a_1 E_p - a_2(1.0 - \exp(-a_3 E_p^{a_4})), \tag{7}$$

where $a_1 = 0.83$, $a_2 = 2.82$, $a_3 = 0.25$, and $a_4 = 0.93$.

3.2.2. Time calibrations

It is necessary to calibrate the TDCs used to measure the neutron's TOF. To facilitate the calibration, a fiber-optic system has been installed in each wall. This system uses an ultraviolet laser to illuminate a bundle of fiber-optic cables simultaneously. The bundle is then separated into individual cables that are fastened to the center of each cell. The fiber-optic cables have been cut to exactly the same length. One extra cable is sent to a small plastic scintillator attached to a fast PMT; this detector provides a constant time reference that is used as the TDC stop signal. In essence, it replaces the fragment detector used for the TOF measurements. By changing the delay between the reference detector and the input to the TDC stop, we obtained different peaks in the TDC spectrum. A composite of such spectra is shown in Fig. 20,

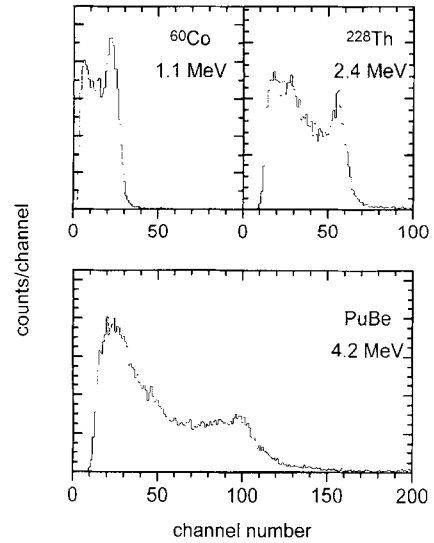

Fig. 19. Pulse-height spectra for three different γ-ray sources. The compton edge is used to obtain a calibration of pulse height to electron equivalent energy for 1.1, 2.4 and 4.2 MeV.
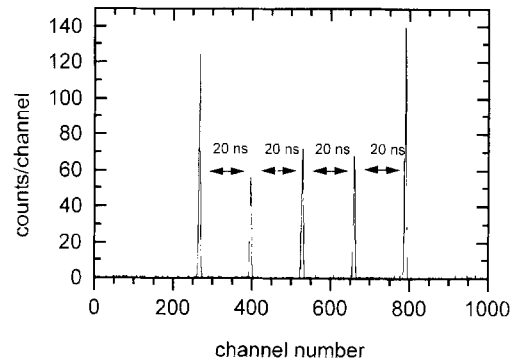

Fig. 20. A laser time calibration for a cell in the Neutron Wall Array. The laser pulses are separated by 20 ns.

where five different laser peaks are present. Knowing the incremental steps added to the delay, we calculate our time-to-channel calibration.

4. The Neutron Wall Array in recent experiments

The Neutron Wall Array was completed in April 1995. To test the simulation models developed by Wang et al. [8], neutrons were detected from the

^{7}Li(p, n)^{7}Be reaction, a reaction that produces only one neutron whose angular distribution and energy distribution are well known. The simulations model the effects of cross talk and out scattering, and they can be easily compared to the results from the ^{7}Li(p, n)^{7}Be experiment. Since its completion, the Neutron Wall Array has been used as intended, i.e., for the study of light, neutron-rich nuclei. In addition, it has been used in a heavy-ion neutron–neutron correlation experiment and in an experiment on nuclear astrophysics. Several more experiments are currently planned.

Acknowledgements

References

[1] I. Tanihata, H. Hamagaki, O. Hashimoto, Y. Shida, N. Yoshikawa, K. Sugimoto, O. Yamakawa, T. Kobayashi, N. Takahashi, Phys. Rev. Lett. 55 (1985) 2676.
[2] D. Sackett et al., Phys. Rev. C 48 (1993) 118.
[3] K. Ieki et al., Phys. Rev. Lett. 70 (1993) 730.
[4] K. Ieki et al., Phys. Rev. C 54 (1996) 1589.
[5] S.J. Gaff, private communication.
[6] J.H. Heltsley, L. Brandon, A. Galonsky, L. Heilbronn, B.A. Remington, A. Vander Molen, J. Yurkon, J. Kasagi, Nucl. Instr. and Meth. A 263 (1988) 441.
[7] R.A. Cecil, B.D. Anderson, R. Madey, Nucl. Instr. and Meth. A 161 (1979) 439.
[8] J. Wang, A. Galonsky, J. Kruse, P. Zecher, F. Deak, A. Horvath, A. Kiss, Z. Seres, K. Ieki, Y. Iwata, Nucl. Instr. and Meth. A 397 (1997) 380.